iScience

CellPress
OPEN ACCESS

Article

Construction and performance analysis of a solar thermophotovoltaic system targeting on the efficient utilization of AM0 space solar radiation

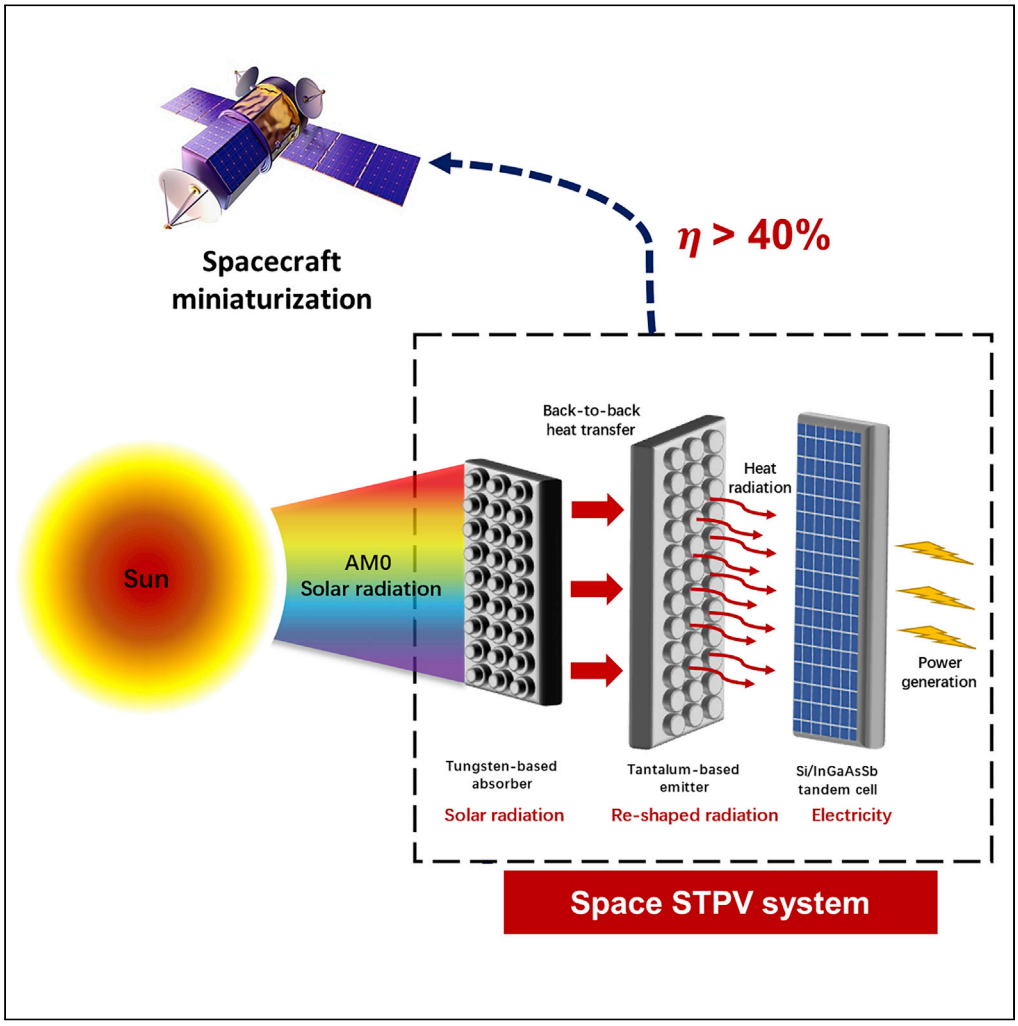

Binghong Chen, Shiquan Shan

shiquan1204@zju.edu.cn

Highlights

A novel space STPV system for AM0 space solar radiation is proposed

Metamaterial structures are designed for spectrum reshaping of AM0 solar radiation

The total absorptance of AM0 radiation is 0.9283 and the TPV efficiency is 51.36

The highest energy conversion efficiency of the space STPV system reaches 40.86

Chen & Shan, iScience 25, 105373
November 18, 2022
https://doi.org/10.1016/j.isci.2022.105373

iScience

CellPress
OPEN ACCESS

Article

Construction and performance analysis of a solar thermophotovoltaic system targeting on the efficient utilization of AM0 space solar radiation

Binghong Chen[1] and Shiquan Shan[2,3,*]

SUMMARY

Solar thermophotovoltaic (STPV) has great potential as efficient power supply source for spacecraft to meet the demand of spacecraft miniaturization. In this work, a novel space STPV system is proposed to achieve the efficient utilization of the AM0 space solar radiation. Metamaterial structures were designed and FDTD method is used to analyze their radiation regulation mechanism. A multi-layer cylindrical periodic structure is used as the absorber which realizes a total absorptance of 0.9283 to AM0 radiation. A cylindrical periodic structure is used as the emitter to reshape the broadband thermal radiation as narrowband to match with the Si/InGaAsSb tandem cell, which realizes a highest TPV efficiency of 51.36%. System performance analysis is conducted and the system presents a highest STPV efficiency of 40.86% and good adaptability under wide range of operating parameters, which reveals its great potential to realize the efficient utilization of AM0 solar radiation for space power supply.

INTRODUCTION

With the rapid development of aerospace science and technology, space utilization has become an important direction to expand human living space. By launching various spacecraft, human beings have achieved near-earth, far-earth, and even deep space exploration. For a spacecraft, power supply is the key to ensure their efficient and stable operation.[1] At present, space power supply sources mainly include chemical energy,[2] nuclear energy,[3] solar energy,[4] etc. Among them, chemical energy and nuclear energy need to be realized by carrying heavy raw materials before launching. For long-term operation tasks, it will cause the problem of heavy preload and is seen as a great application limitation. In contrast, solar energy has the characteristics of abundant reserves and sustainable replenishment in space, which is an unparalleled advantage especially for the space exploration tasks in the solar system.[5] Currently, photovoltaic (PV) has been applied in space energy supply, which can ensure the stable operation of spacecraft for several years.[6] However, the efficiency of single p-n cell is limited to around 30% without considering radiation loss due to the existence of the Shockley-Queisserlimit.[7] Under this technical background, in order to meet the power supply requirements of the spacecraft, large PV cell area needs to be set up to increase the system energy input, thereby increasing the self-loading and the external volume of the spacecraft. Besides, the unutilized long-band radiation will also lead to the temperature rise-up of the PV cell, thereby reducing its operating performance. Multi-junction PV is brought out to broaden the usable wavelength range by integrating different PV cells, thus increasing the conversion efficiency of solar radiation. Currently, the highest efficiency of space multi-junction PV system is reported to be 34.2%.[8] However, the multi-junction PV system needs to be coupled with solar concentrators to increase the output energy density but direct concentration of solar radiation on the PV cell could lead to local overheat which might damage the PV cell and threaten the operation stability. In order to solve this problem, a cooling system is required,[9]which further worsens the self-loading problem. In addition, the exposure of the PV cell also limits its application in space exploration with extreme environment. Therefore, new technology needs to be developed to overcome the shortage of the existing technology and realize the efficient and stable utilization of AM0 radiation to meet the power supply requirement of spacecraft.

Thermophotovoltaic (TPV) is a novel technology proposed in recent years, which outstands for the high energy conversion efficiency to effectively break through the Shockley-Queisserlimit.[10,11] At present,

[1]School of Energy and Power Engineering, University of Shanghai for Science and Technology, Shanghai 200093, China

[2]State Key Laboratory of Clean Energy Utilization, Zhejiang University, Hangzhou 313003, China

[3]Lead contact

*Correspondence: shiquan1204@zju.edu.cn

https://doi.org/10.1016/j.isci.2022.105373

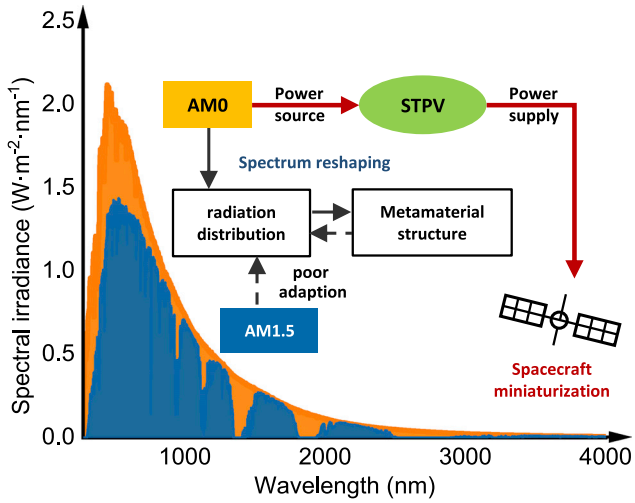

Figure 1. Comparison between AM0 and AM1.5 solar radiation spectra

TPV system for space power supply often uses nuclear energy as heat source.[12] However, the nuclear energy reactor causes the problem of large preload. In contrast, solar TPV (STPV) uses the external solar energy as heat source which can well avoid such problem.[13] Currently, the highest STPV system on ground with AM1.5 solar radiation as heat source is reported to be 41.8%.[14] Such high energy conversion efficiency of STPV is very tempting for space power supply since it can effectively reduce the external radiation receiving area, which can help to reduce the external volume of spacecrafts. Therefore, STPV is a good candidate for space power supply that is worth for further exploration to promote the miniaturization and weight reduction of spacecrafts.

To achieve the efficient utilization of solar energy, a selective absorber and emitter with ideal radiation properties needs to be included in the STPV system. Thanks to the development of micro-nano technology, metamaterial structures are artificially designed and utilized in TPV systems to realize the effective spectrum reshaping.[15]Qiu et al.[16] designed a perfect selective metamaterial absorber for high-temperature AM1.5 solar energy harvesting, which can achieve a high solar-to-heat efficiency of 92.31%–77.78%. Similarly, nano structures including core-shell nanoparticles[17] pyramidal nanostructures,[18] and nanorings[19] have been proposed to realize the perfect absorption of AM1.5 solar energy as well. On this basis, selective emitters are designed to convert the absorbed energy to thermal radiation and match with the PV cells. Jiang et al.[20] designed a multi-layer ring metamaterial structure which can reshape the thermal radiation to reach a spectral efficiency of 85.6% at 1600 K. These works prove the effectiveness of metamaterial structures in STPV systems, which provides important inspirations for the construction of space STPV system. However, current STPV studies focus on the utilization of AM1.5 near-ground solar energy,[21]which has different radiation distribution characteristics from AM0 space solar radiation (Blackbody spectrum). The two typical solar radiation spectra are compared in Figure 1. As is seen, AM0 radiation present as a continuous distribution with greater radiation intensity. This will change the thermal balance of the absorber and further influence the performance of the STPV system, which leads to the poor adaptability of the existing metamaterial structures to the utilization of AM0 space solar radiation. Therefore, in order to realize efficient utilization of space solar energy, it is necessary to take the distribution characteristics of AM0 solar radiation into consideration and design simple and reliable metamaterials to construct an effective space STPV system. This system can realize the efficient utilization of AM0 space solar radiation and lay a solid foundation for the miniaturization of spacecrafts.

Concerning the above background, this work targets on the efficient utilization of AM0 space solar radiation with STPV.Metamaterial radiation regulation structures including a selective absorber and emitter are designed based on the distribution characteristics of AM0 solar radiation spectrum. On this basis, a space STPV system is constructed and detailed analysis is conducted to obtain the operation performance of the proposed system in realizing the efficient utilization of AM0 space solar radiation. The development potential of the space STPV system is pointed out, so as to provide theoretical support for the practical application of STPV in space power supply.

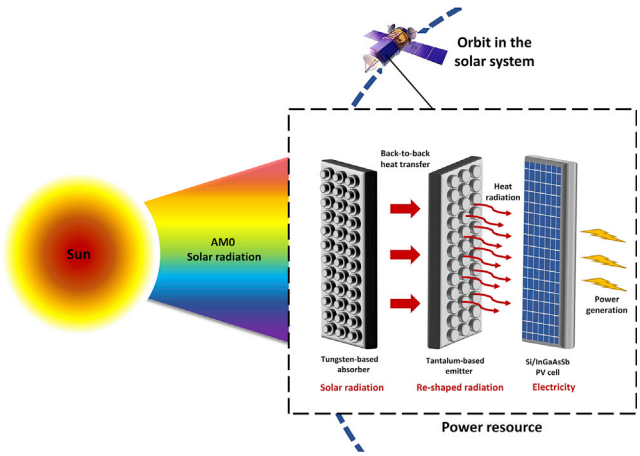

Figure 2. Schematic diagram of the space STPV system

RESULT AND DISCUSSION

Overview of the space STPVsystem

Based on the demand for miniaturized space power supply, a novel space STPV system based on metamaterial spectral regulation is proposed, as shown in Figure 2, which is mainly composed of an absorber, an emitter, and a PV cell. Considering the operating area of the target spacecraft, AM0 solar spectrum is used as the solar radiation distribution,[22] which serves as the energy input for the system. The AM0 solar radiation is concentrated and then absorbed by the selective absorber and converted to heat energy. The heat is transferred through the back-to-back arrangement structure to the selective emitter, which then generates selective radiation to the PV cell and generates electricity output, thereby realizing efficient heat-electric conversion. In order to enhance the energy utilization efficiency, a Si/InGaAsSb tandem cell is used in this system. By introducing a metamaterial selective absorber and emitter with ideal absorptance/emittance distribution, AM0 radiation is absorbed and reshaped as a selective radiation spectrum to match with the PV cell, thereby improving the energy conversion efficiency of the system to meet the power supply requirement of small spacecraft.

Solar radiation absorption

To maximize the energy input of the system, a selective absorber with high absorption efficiency of AM0 solar radiation should be obtained first, which can efficiently convert the solar energy into heat and lay a solid foundation for the further utilization by the backend of the system. Accordingly, a multi-layer cylindrical periodic structure is designed. It is mainly composed of tungsten (W), which has high melting point of 3422 °C[23] and presents good stability at high temperature[24] and Al_2O_3 is used as the dielectric layer.[25] The specific structure and main geometrical parameters are shown in Figure 3. The proposed structures can be fabricated with the following ways: First, a W film is deposited on a substrate and an E-beam resist is spin coated upon it. Then, electron beam lithography is used to fabricate a circular hole on the resist. After that, a W film is deposited by magnetic sputtering to fill the hole

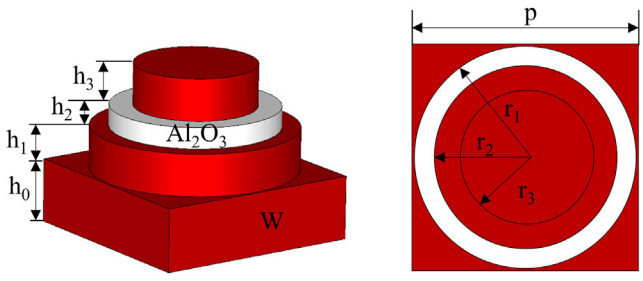

Figure 3. Structure diagram of the selective absorber

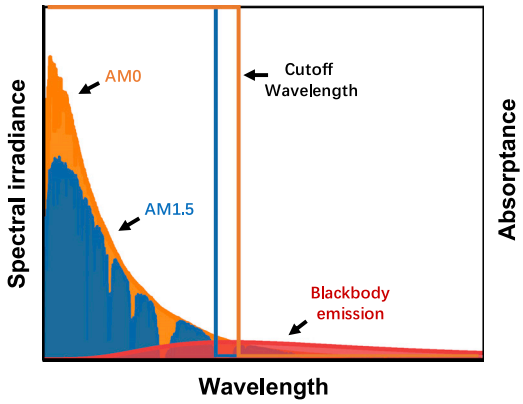

Figure 4. Influence of solar radiation distribution on the ideal absorptance distribution of the absorber

and the resist layer is lifted off afterward to obtaine the first layer of W cylinder. Afterward, similar step is repeated and Al_2O_3 and W are deposited in sequence to form the layer 2 and layer 3 of cylinder to obtain the proposed multi-layer cylinder structure. The roughness of magnetic sputtering and electron beam lithography can reach <5 nm,[26,27] which can well meet the demand of manufacturing the proposed structures.

Compared with near-ground STPV system, the key difference of the space STPV system is the input solar radiation distribution as it appears to be with higher intensity and continuous distribution. According to Equation 11 in method details, the relative intensity of the blackbody emission and the concentrated solar radiation is a key factor that determines the absorption efficiency of solar radiation. To obtain the optimal performance, the absorptance distribution of an ideal absorber should be as close to 1 as possible at the wave band where the concentrated solar radiation intensity is higher than the radiation heat loss, and be close to 0 at the wave band where the concentrated solar radiation intensity is lower than the radiation heat loss, as is shown in Figure 4. The wavelength where absorptances changes from 1 to 0 is defined as cutoff wavelength. As is seen from the figure, AM0 appears to have higher and continuous distribution in the long band range while AM1.5 presents defects in 1800–1950 nm, which clearly changes the relative ratio of the two radiation in the long band range. Therefore, the cutoff wavelength of the absorber should be longer than the existing absorber for AM1.5 absorption to obtain the optimal absorption of the AM0 radiation and a new design of absorber is needed.

Based on the above analysis, the geometric parameters of the proposed metamaterial absorber are comprehensively optimized to achieve the efficient absorption of AM0 radiation. The optimal parameter combination is obtained as: p = 500 nm, r_1 = 245 nm, r_2 = 200 nm, r_3 = 145 nm h_0 = 150 nm, h_1 =100 nm, h_2= 50 nm, h_3 = 100 nm. Under this combination, a total absorptance of 0.9283 to the AM0 solar radiation is obtained. The specific absorptance distribution of the absorber is shown in Figure 4. It can be seen that the absorptance of the absorber in the region below 2000 nm is close to 1, so that sufficient absorption of the solar radiation in this region can be achieved. When the wavelength is above 2000 nm, the absorptance drops rapidly. In this region, the intensity of concentrated solar radiation is low and the intensity of radiation heat loss of the absorber is high. Therefore, reducing the emittance/absorptance of the absorber in this region can effectively reduce the radiation heat loss, thereby ensuring the high absorption efficiency of the AM0 solar radiation. The AM0 solar radiation spectrum before and after absorption by the selective absorber is compared and shown in Figure 5. It can be found that the solar radiation in the wave band below 2000 nm is fully absorbed by the selective absorber while the solar radiation at the wave band above 2000 nm is abandoned considering the comparatively stronger radiation heat loss in this region.

The effective impedance theory[28] is used to analyze the absorption mechanism of the selective absorber. The relation between the effective impedance and absorptance can be expressed as:

$$\alpha_\lambda = \frac{4Re(Z)}{[1+Re(Z)]^2+[Im(Z)]^2}$$

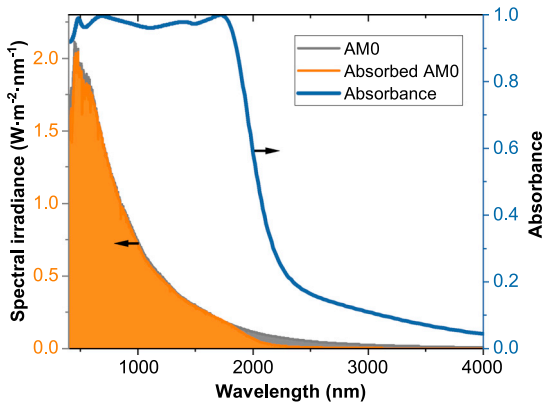

Figure 5. The absorptance distribution and absorption effect of the absorber on AM0 radiation

Accordingly, the effective impedance Z of the absorber is calculated and shown in Figure 6. It can be seen that at the wave band below 2000 nm, the real part of the effective impedance of the absorber is close to 1 and the imaginary part *Im*(*Z*) is close to 0. This is similar to the effective impedance of the free space, which means that the impedance of the absorber is highly matched with the free space. According to the above equation, the absorptance at the wavelength λ is therefore close to 1, indicating the high absorptance at corresponding wavelength. As a result, the reflection of the incident waves by the absorber is greatly reduced in this region, so that the absorber can fully absorb the solar radiation in the wave band below 2000 nm. When the wave band is above 2000 nm, the real part *Re*(*Z*) and the imaginary part *Im*(*Z*) of the effective impedance deviate from 0 to 1 rapidly, indicating that the matching degree between the absorber and the free space impedance decreases rapidly. As a result, the absorptance/emittance of the absorber decreases rapidly, thereby effectively reducing the radiation heat loss of the absorber in this wave band and improving the solar absorption efficiency of the absorber.

To further analyze the selective absorption mechanism of the absorber, the distribution of electric field |**E**| and magnetic field |**H**| in the absorber under incident waves with different wavelengths is obtained and shown with a cross-sectional view in Figure 7. It can be seen that when the wavelength is short, strong |**E**| and |**H**| appears at the small gap between periodic structures at the bottom part, which is introduced by the local surface plasmon resonance (LSPR). This indicates that the absorption of the short-band radiation is mainly realized with the bottom part of the absorber by the excitation of LSPR. When the wavelength increased to above 1500 nm, the effect of LSPR gradually weakens. The response location moves to the upper part of the absorber. It can be observed that strong |**H**| appears within the dielectric layer with intensified |**E**| at the left and ride sides, which is due to the magnetic polaritons (MPs). This indicates that the absorption of long-band radiation is mainly realized with the upper part of the absorber by MPs.

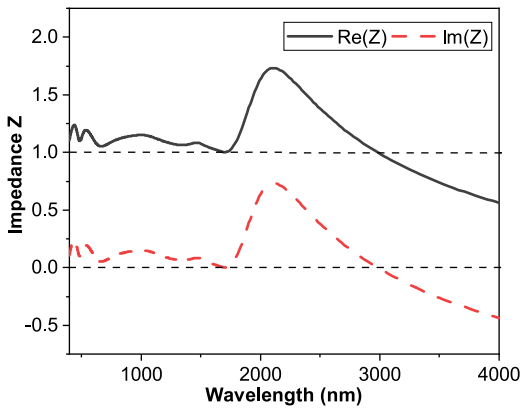

Figure 6. The effective impedance of the selective absorber under different wavelengths

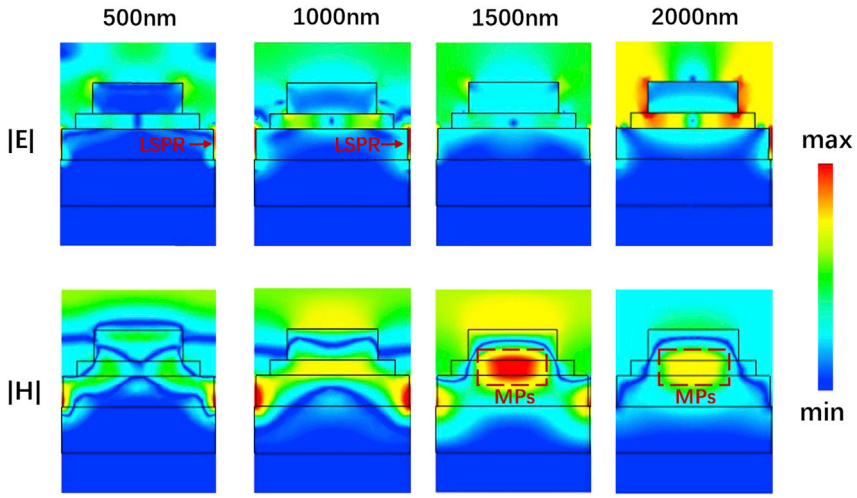

Figure 7. The |E| field and |H| field distribution in the selective absorber under incident waves with different wavelengths

Therefore, it can be obtained that the high absorption to AM0 radiation of the proposed absorber is realized with the combined effect of LSPR and MPs excited in different part of the absorbers.

In order to evaluate the overall operation performance of the absorber, the absorption efficiency η_{abs} of AM0 radiation under different concentration ratios and operating temperatures is obtained and shown in Figure 8. As can be seen, as the operating temperature increases, the absorption efficiency decreases. This is because as the temperature of the absorber increases, the thermal radiation spectrum of the absorber shifts to the short band, and its overlapping area with the solar radiation increases. In addition, as the temperature increases, the intensity of the thermal radiation increases as well. Since the absorptance/emittance is relatively high in this region, the thermal heat loss will increase due to the combined effect of the above two factors, which leads to a decrease in the absorption efficiency. Comparing the solar absorption efficiency of the absorber under different concentration ratios, it can be found that with the increase of the concentration ratio, the absorption efficiency gradually increases, and when the operating temperature of the absorber is higher, the increase of the absorption efficiency is more obvious. This is because with the increase of the concentration ratio, the input energy of solar radiation increases significantly while the radiation heat loss of the absorber remains unchanged. Therefore, the ratio of radiation heat loss to the total input energy decreases significantly, so the adverse effect of the radiation heat loss is reduced. However, when the temperature is low, the effect of improving the concentration ratio is not obvious. It can be seen from the figure that at 1000 K, the absorption efficiency of the absorber is maintained above 92% under different concentration ratios. This is because at this temperature range, the

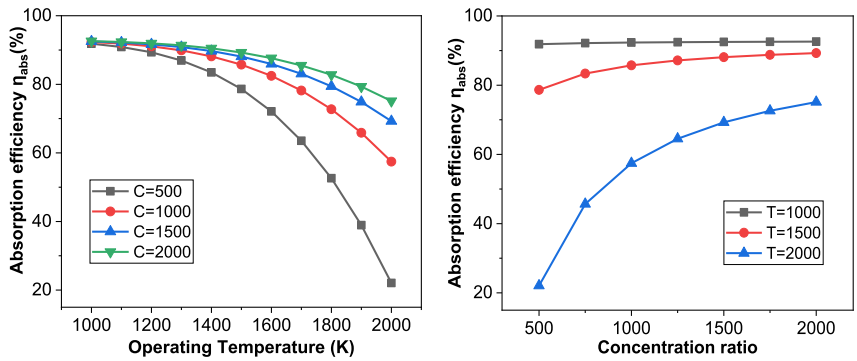

Figure 8. Absorption efficiency of the selective absorber under different operating parameters

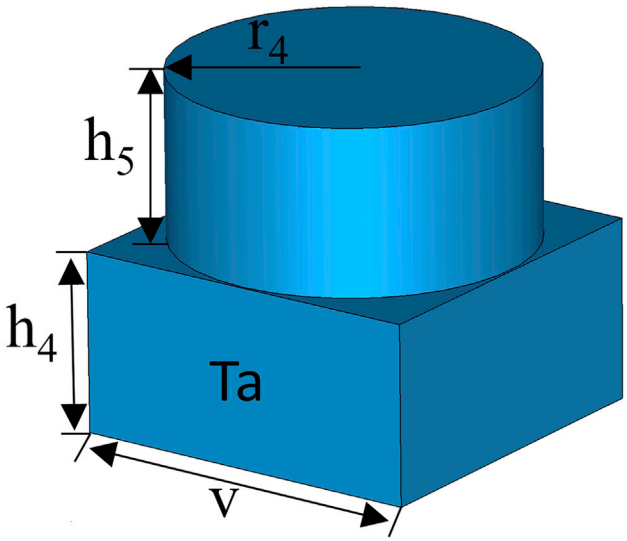

Figure 9. Structure diagram of the selective emitter

radiation heat loss is very small so its adverse effect is very limited. Therefore, when the operating temperature of the absorber is low, a low concentration ratio can already maintain a good absorption efficiency. When the operating temperature is high, however, a high concentration ratio is necessary since the radiation heat loss at this temperature range cannot be neglected. As can be seen from the figure, at 2000 K, when the concentration ratio increases from 500 to 2000, the absorption efficiency of the absorber increases drastically from 22.08% to 75.14%, which is an obvious improvement. The high concentration ratio can be realized with a proper arrangement of Fresnel lens in front of the absorber, which is proven effective in achieving a concentration ratio up to 4300.[29] As a whole, increasing the operating temperature of the absorber will lead to a significant increase in its radiation heat loss, which is not conducive to the solar absorption efficiency of the absorber, while increasing the concentration ratio can alleviate this problem to a certain extent.

TPV heat-electric conversion

After the solar absorption of the absorber, the heat is transfer to the emitter which emits thermal radiation to be utilized by the PV cell and generate electric power. According to the external quantum efficiency (EQE) distribution of the Si/InGaAsSb tandem cell, photons with wavelengths above the cutoff wavelength of the PV cell cannot be utilized so this portion of radiation is defined as inconvertible. In addition, it has been pointed out that broadband emitters lead to the energy waste of short-band photons and the temperature rise-up problem of the PV cell.[30] Therefore, a narrowband selective emitter with high matching degree with Si/InGaAsSb tandem cell will be an ideal emitter for the system to enhance the TPV efficiency. To achieve this, a simple cylindrical metamaterial periodic structure is designed. The emitter is made of metal tantalum, which has a melting point of 3017°C to ensure the stability in the target operating temperature range and has been commonly used to construct narrowband emitters due to its inherent radiation characteristics.[14] The specific structure and geometrical parameters of the emitter are shown in Figure 9. The geometrical parameters are further optimized to obtain the optimal TPV power generation performance. The structure can be fabricated with similar way of the absorber.

Based on the EQE characteristics of the Si/InGaAsSb tandem cell, the optimal geometric parameter combination of the emitter is obtained as: v = 395 nm, r_4 = 195 nm, h_4 = 200 nm, h_5 = 185 nm. The emittance distribution of the emitter is shown in Figure 10. As is seen, the obtained emitter is a typical narrowband emitter with an emittance peak around 2000 nm. It can be found that the peak wavelength is slightly shorter than the cutoff wavelength of the Si/InGaAsSb tandem cell. Using this structure as the emitter, the thermal radiation emitted by the emitter can be concentrated in this wave band, thereby reducing unnecessary photon energy waste and the ratio of the inconvertible energy in the long band.

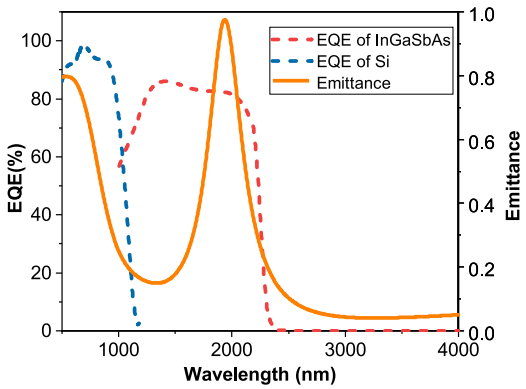

Figure 10. Emittance distribution of the emitter and the EQE curve of Si/InGaAsSb tandem cell

To show the effect of the selective emitter, the radiation spectrum generated by a blackbody emitter and the obtained selective emitter is compared in Figure 11. It can be seen from the figure that when a blackbody emitter is used, the radiation spectrum is a typical broadband radiation, and a large portion of the radiation is in the wave band above the cutoff wavelength where the photons cannot be utilized by the PV cell, which severely lowers the energy utilization efficiency and leads to the temperature rise-up problem of the PV cell as well. When the proposed selective emitter is used, it can be found that the broadband blackbody radiation is effectively reshaped to a narrowband radiation. The proportion of inconvertible radiation energy is greatly reduced, which means that most of the radiation energy can be effectively converted to electricity by the PV cell. Therefore, a great enhancement of the energy conversion efficiency can be expected. In addition, it can be found that the radiation of the selective emitter concentrates in the region with wavelength slightly longer than the cutoff wavelength of the PV cell. Since one photon can only excite one electron pair during the operation of the PV cell, when the photon wavelength is slightly shorter than the cutoff wavelength of the PV cell, its energy can be utilized to the greatest extent.[31] Therefore, the spectrum reshaped by the selective emitter can effectively improve the energy conversion efficiency.

To explore the radiation regulation mechanism of the selective emitter, the electric field (|**E**|) and magnetic field (|**H**|) distribution within the emitter under the action of incident wave at the emittance peak wavelength 2000 nm are analyzed, and the results are shown in Figure 12. As is marked with dash line in the figure, the left one shows the cross-section distribution in the vertical plane at the edge of the periodic structure and the right one shows the cross-section distribution in the horizontal plane across the height with the strongest |**E**| or |**H**| distribution. It can be found from the upper figure that the distribution of the |**E**| presents with strong intensity in two zone around the narrowest gap between the two periodic structures in the top with a direction from left to right. As is seen in the bottom figure, the |**H**| presents with strong intensity in the gap in the bottom with a direction vertical to the |**E**|. This phenomenon indicates that a strong electromagnetic field is generated in the gap.[32] According to this space distribution, it can be inferred that LSPR are excited within the nanogap under the action of incident wave

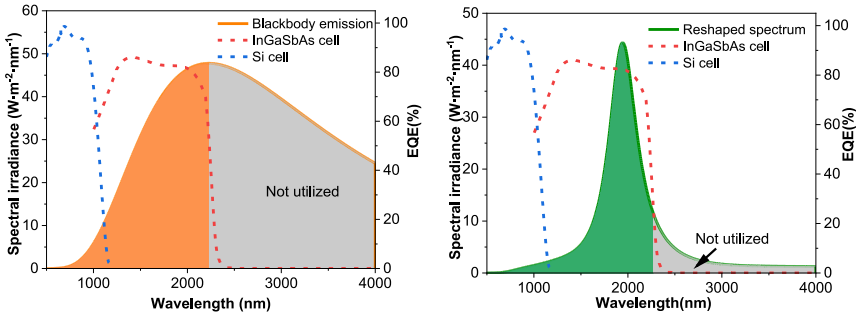

Figure 11. The available spectral range of a blackbody emitter and the selective emitter

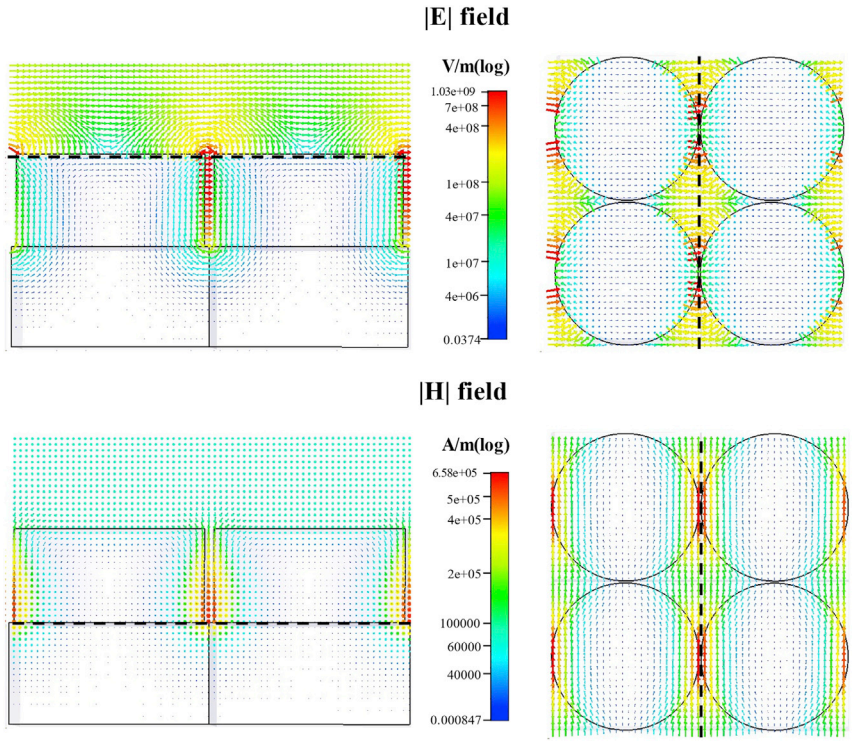

Figure 12. The |E| field and |H| field distribution in the selective emitters under incident waves with a wavelength of 2000 nm

with a wavelength of 2000 nm.[33] Under the effect of LSPR, the incident wave with wavelength around 2000 nm is dissipated due to ohmic dissipation, therefore leading to the selective radiation characteristic of the emitter to realize the radiation regulation of thermal radiation spectrum and achieve efficient conversion of the absorbed AM0 solar energy.

In order to evaluate the influence of operating parameters on the TPV heat-electric conversion part, the TPV performance of the backend of the system (selective emitter-PV cell) under different operating temperatures is further explored. First, from the perspective of spectral utilization, based on the EQE curve of the Si/InGaAsSb tandem cell, 2235 nm is defined as the cutoff wavelength and the spectral efficiency of the emitter radiation is statistically obtained. The results are shown in Figure 13. It can be seen that by introducing the selective emitter, the spectral efficiency is increased for 2.795 times from 27.01% to 75.50% at 1000 K. When the operating temperature is 2000 K, the spectral efficiency can reach up to 92.92%. It can be seen that the introduction of the selective emitter can greatly increase the proportion of convertible radiation and the improvement effect is more obvious at low temperatures. This is because thermal radiation has a broadband distribution in the whole wavelength range, and the lower the temperature, the more the radiation peak is inclined to the long band. By introducing a narrowband selective emitter, the inconvertible long-band radiation can be effectively filtered out, thereby increasing the proportion of the convertible radiation energy of the emitter and lay a good foundation for the improvement of the performance of the PV cell.

Furthermore, the TPV efficiency and the energy flux of the generated electricity at different operating temperatures were calculated, and the obtained results are shown in Figure 14. It can be seen that in the range of 1000–2000 K, with the increase of temperature, the energy conversion efficiency increases from 32.79% to 51.36%, and the energy flux increases from 1.52 $kW \cdot m^{-2}$ to 113.11 $kW \cdot m^{-2}$. This is because, as the temperature increases, the proportion of convertible radiation gradually increases, so that more radiation energy can be effectively converted to electricity, thereby improving the TPV efficiency. Therefore, as far as the TPV conversion end is concerned, the higher the operating temperature is, the more favorable it is to improve the energy conversion efficiency.

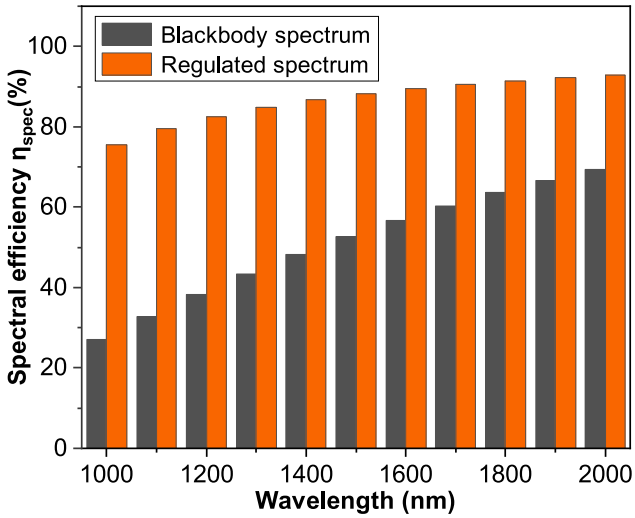

Figure 13. Spectral efficiency of the radiation spectrum

Performance analysis of the overall system

After obtaining the metamaterial structures with desirable radiation characteristics based on the single end performance analysis, the space STPV system is constructed and the structure layout is shown in Figure 15. As is seen, the absorber and emitter are arranged back-to-back with the same temperature. An IR heat shield is set up on the backside of the emitter to reflect the thermal radiation of the emitter to reduce the heat loss.[34] Since the heat flux of the emitter is lower than the solar radiation energy flux of the absorber, the area of the absorber is smaller than that of the emitter to maintain the thermal equilibrium of the system. This structure is conducive to reduce the external volume of the spacecraft because only the small area of the absorber should be set outside the spacecraft while the large area part can be hidden in the inner part of the spacecraft, which is good news for the miniaturization of spacecraft.

From the above single-end analysis results, it can be found that the operating temperature has opposite effect on the performance of solar absorption and TPV conversion, and increasing the concentration ratio can effectively overcome the problem of low absorption efficiency of the absorber at high temperature. Since the absorber and the emitter maintain the same operating temperature during the operation process, to maximize the energy conversion efficiency of the system, it is necessary to consider the influence of different operating parameters on the overall STPV system efficiency to obtain the optimal operating parameters for the system. The STPV system efficiency under different operating parameters is calculated and obtained, and the results are shown in Figure 16. It can be found that when the concentration ratio is

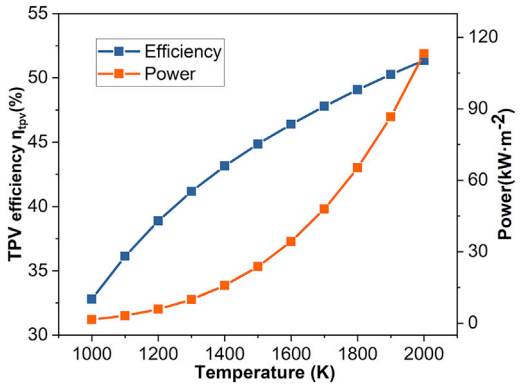

Figure 14. Energy conversion efficiency and the generated power density

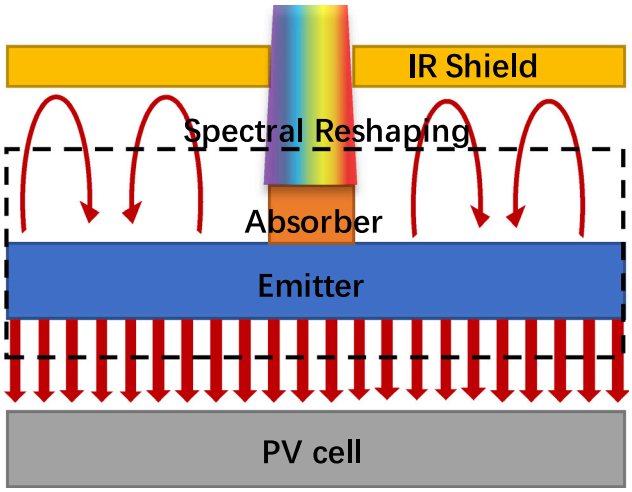

Figure 15. Structure layout of the space STPV system

constant, with the increase of temperature, the STPV system efficiency shows a trend of first increasing and then decreasing. This is because when the temperature is low, although the absorber efficiency is high, the spectral efficiency of the emitter is low so only a small portion of the energy is converted into electricity by the PV cell. As a result, the overall energy conversion efficiency of the system is low. However, when the temperature is too high, the absorber suffers from significant radiation heat loss. This greatly reduces the energy input of the system and has an adverse effect on the overall efficiency of the system as well. When the temperature is within an appropriate range, the radiation heat loss of the absorber and the loss of convertible energy ratio of the emitter are balanced, and the system efficiency reaches its highest. In addition, by comparing the STPV system efficiency under different concentration ratios, it can be found that with the increase of the concentration ratio, the optimal operating temperature increases, and the corresponding optimal STPV system efficiency is also improved. This is because improving the solar concentrating ratio can effectively reduce the effect of radiation heat loss of the absorber, thereby enabling the system to operate at higher temperatures and achieving higher system efficiency. It can be seen from the figure that when the concentration ratio is 2000, the system can reach the highest STPV system efficiency of 40.86% at 1700 K, which is comparable to the STPV efficiency record with AM 1.5 of 41.8% on ground. In addition, in the operating temperature range of 1500 K–1800 K, the system efficiency remains

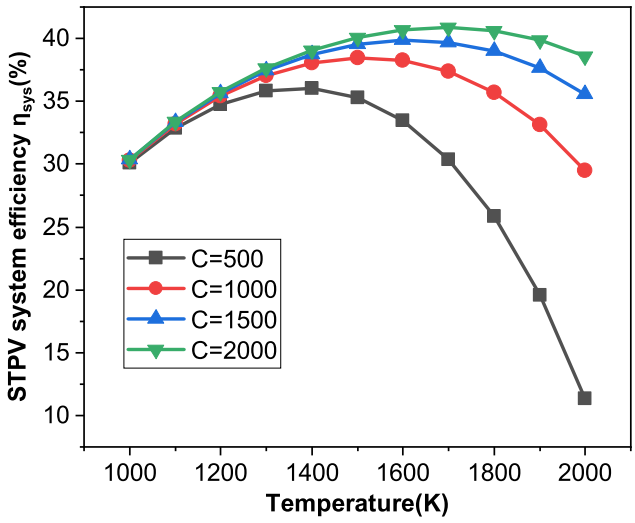

Figure 16. The STPV system efficiency of the space STPV system under different operating parameters

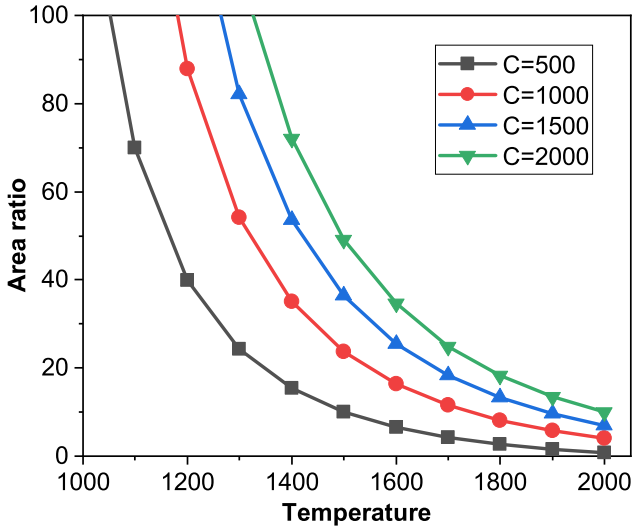

Figure 17. The area ratio of absorber and emitter under different operating parameters

above 40%, which is significantly higher than common PV system as well as the existing record of space multi-junction system. The maintenance of high temperature can be realized with the use of thermal insulation material such as silicon carbide.[35] Besides, even under low concentration ratio of 500, the system efficiency still remains in the range of 30%–35% at temperature 1000 K–1700 K, which also demonstrates the adaptability of the system to a wide range of operating parameters. Therefore, it can be concluded that the efficient utilization of the AM0 solar radiation can be achieved with the proposed space STPV system.

On this basis, the structure arrangement of the system is discussed as well. As is pointed out above, the relatively smaller area of the absorber is beneficial for small spacecrafts. However, the area ratio of the absorber to the emitter cannot be too large considering the structural rationality of the system. Considering the different energy flux of the absorber and the emitter with their back-to-back arrangement, their area ratio $\frac{A_{abs}}{A_{emi}}$ is calculated and the results are shown in Figure 17. It can be seen from the figure that the area ratio of the absorber and the emitter gradually decreases with the increase of temperature. When the temperature is low, the area of the absorber is significantly smaller than that of the emitter. This is because the radiation intensity of the emitter is significantly affected by the temperature. When the temperature is low, the thermal radiation of the emitter is very weak so a very large area is required at the emitter end. In addition, when the concentration ratio of the absorber is large, the input energy of the absorber is obviously increased, so that the emitter requires a larger area to emit the heat. However, the emitter area cannot be too large since it is not conducive to the realization of the device. Therefore, the area ratio should be controlled within a reasonable range by increasing the temperature and selecting a proper concentration ratio.

To select an appropriate operating parameters combination, it is necessary to comprehensively consider the system efficiency and area ratio, as well as the concentrating structure, so as to effectively optimize the overall performance and structural achievability of the space STPV system. Combined with the above calculation results, the highest system efficiency can be reached under the operating parameters of 1700 K and the concentration ratio of 2000. The area ratio of the absorber and the emitter is about 24.93, which is reasonable and can be realized by internally expanding the area through various forms such as spiral distribution. Combined with the high energy conversion efficiency and reasonable radiant receiving area, the space STPV system can realize efficient utilization of AM0 space solar energy and provide efficient power supply for the spacecraft with relatively small radiation receiving area, which is of great significance to the development of the miniaturization of spacecraft and is a promising energy supply method for the future space utilization.

Conclusions

In this work, a space STPV system is constructed to achieve the efficient utilization of the AM0 space solar radiation to serve as a potential power supply for small spacecrafts. In order to reshape the AM0 solar spectrum, a metamaterial selective absorber and emitter are designed. FDTD method is used to calculate the

radiation characteristics of the micro-nano structures and their radiation regulation mechanism is analyzed. Single-end and overall system performance analysis are conducted to obtain the optimal operating parameters considering the influence of operating parameters and the structural rationality. The main conclusions are as follows:

1) A selective absorber made of W and Al_2O_3 with a multi-layer cylindrical periodic structure is constructed to achieve the efficient absorption of the AM0 solar radiation. The optimized structure presents a total absorptance of 0.9283, which can fully absorb the radiation in the band below 2000 nm and reduce the radiation heat loss at 2000–3000 nm.
2) A selective Ta emitter with a cylindrical periodic structure is constructed. It presents a narrowband emittance distribution with a peak around 2000 nm, which is highly matched with the Si/InGaAsSb tandem cell. With the introduction of the selective emitter obtained, the highest spectral efficiency and TPV conversion efficiency can reach 92.92% and 51.36% at 2000 K, respectively.
3) The operating temperature has opposite influence on the performance of solar absorption and TPV conversion. As the temperature increases, the absorber suffers from severe radiation heat loss leading to the decrease of its solar absorption efficiency decrease while the radiation intensity and convertible energy ratio of the emitter increases leading to the increase of the TPV conversion efficiency.
4) Considering the thermal equilibrium of the absorber and emitter as well as the overall energy conversion characteristics, the highest efficiency of the system is determined to be 40.86% at 1700 K with a concentration ratio of 2000. The absorber-emitter area ratio is 24.93, which can be realized with the internal spiral structure.

Limitations of the study

This work reveals the application potential of solar thermophotovoltaic in space power supply to realize efficient solar energy conversion. The comparatively high cost of metamaterial fabrication is the current limit of the system and is expected to be overcome with future development of micro-nano fabrication technology.

STAR★METHODS

Detailed methods are provided in the online version of this paper and include the following:

- KEY RESOURCES TABLE
- RESOURCE AVAILABILITY
  - Lead contact
  - Materials availability
  - Data and code availability
- METHOD DETAILS
  - Radiation characteristics calculations
  - Performance analysis

ACKNOWLEDGMENTS

This work was supported by National Natural Science Foundation of China (CN) (52106178), the National Postdoctoral Program for Innovative Talents of China (CN) (BX2021254) and China Postdoctoral Science Foundation (2021M702793).

AUTHOR CONTRIBUTIONS

B.C.: Conceptualization, Methodology, Investigation, Writing-Original Draft. S.S.: Writing-Review & Editing, Supervision, Project Administration, Funding Acquisition.

DECLARATION OF INTERESTS

The authors declare no competing interests.

Received: July 22, 2022
Revised: September 25, 2022
Accepted: October 13, 2022
Published: November 18, 2022

REFERENCES

1. Zhang, T., Li, Y., Chen, Y., Feng, X., Zhu, X., Chen, Z., Yao, J., Zheng, Y., Cai, J., Song, H., and Sun, S. (2021). Review on space energy. Appl. Energy *292*, 116896. https://doi.org/10.1016/j.apenergy.2021.116896.

2. Sone, Y., Ueno, M., and Kuwajima, S. (2004). Fuel cell development for space applications: fuel cell system in a closed environment. J. Power Sources *137*, 269–276. https://doi.org/10.1016/j.jpowsour.2004.03.051.

3. El-Genk, M.S. (2008). Space nuclear reactor power system concepts with static and dynamic energy conversion. Energy Convers. Manag. *49*, 402–411. https://doi.org/10.1016/j.enconman.2007.10.014.

4. Cardinaletti, I., Vangerven, T., Nagels, S., Cornelissen, R., Schreurs, D., Hruby, J., Vodnik, J., Devisscher, D., Kesters, J., D'Haen, J., et al. (2018). Organic and perovskite solar cells for space applications. Sol. Energy Mater. Sol. Cells *182*, 121–127. https://doi.org/10.1016/j.solmat.2018.03.024.

5. Jaffe, P., and McSpadden, J. (2013). Energy conversion and transmission modules for space solar power. Proc. IEEE *101*, 1424–1437. https://doi.org/10.1109/JPROC.2013.2252591.

6. Luque, A., and Hegedus, S. (2011). Handbook of Photovoltaic Science and Engineering (John Wiley & Sons, Ltd), pp. 546–599. https://doi.org/10.1002/9780470974704.

7. Ehrler, B., Alarcón-Lladó, E., Tabernig, S.W., Veeken, T., Garnett, E.C., and Polman, A. (2020). Photovoltaics reaching for the shockley–queisser limit. ACS Energy Lett. *5*, 3029–3033. https://doi.org/10.1021/acsenergylett.0c01790.

8. France, R.M., Geisz, J.F., Song, T., Olavarria, W., Young, M., Kibbler, A., and Steiner, M.A. (2022). Triple-junction solar cells with 39.5% terrestrial and 34.2% space efficiency enabled by thick quantum well superlattice. Joule *6*, 1121–1135. https://doi.org/10.48550/arXiv.2203.15593.

9. Radwan, A., Ahmed, M., and Ookawara, S. (2016). Performance enhancement of concentrated photovoltaic systems using a microchannel heat sink with nanofluids. Energy Convers.Manag. *119*, 289–303. https://doi.org/10.1016/j.enconman.2016.04.045.

10. Shan, S., Tian, J., Chen, B., Zhang, Y., and Zhou, Z. (2022). Comparison between spectrum-split conversion and thermophotovoltaic for solar energy utilization: thermodynamic limitation and parametric analysis. Energy Convers.Manag. *255*, 115331. https://doi.org/10.1016/j.enconman.2022.115331.

11. Teofilo, V.L., Choong, P., Chang, J., Tseng, Y.L., and Ermer, S. (2008). Thermophotovoltaic energy conversion for space. J. Phys. Chem. C *112*, 7841–7845. https://doi.org/10.1021/jp711315c.

12. Nakamura, T., and Smith, B. (2012). Space solar energy system for thermal and photosynthetic applications. AIAAJ. https://doi.org/10.2514/6.2012-5169.

13. Chubb, D.L., Good, B.S., and Lowe, R.A. (1996). Solar thermophotovoltaic (STPV) system with thermal energy storage. AIP Conf. Proc. *358*, 181. https://doi.org/10.1063/1.49686.

14. Rana, A.S., Zubair, M., Danner, A., and Mehmood, M.Q. (2021). Revisiting tantalum based nanostructures for efficient harvesting of solar radiation in STPV systems. Nano Energy *80*, 105520. https://doi.org/10.1016/j.nanoen.2020.105520.

15. Shan, S., Chen, C., Loutzenhiser, P.G., Ranjan, D., Zhou, Z., and Zhang, Z.M. (2020). Spectral emittance measurements of micro/nanostructures in energy conversion: a review. Front. Energy *14*, 482–509. https://doi.org/10.1007/s11708-020-0693-0.

16. Qiu, Y., Zhang, P., Li, Q., Zhang, Y., and Li, W. (2021). A perfect selective metamaterial absorber for high-temperature solar energy harvesting. Sol. Energy *230*, 1165–1174. https://doi.org/10.1016/j.solener.2021.11.034.

17. Wang, Z., Quan, X., Zhang, Z., and Cheng, P. (2018). Optical absorption of carbon-gold core-shell nanoparticles. J. Quant. Spectrosc. Radiat. Transf. *205*, 291–298. https://doi.org/10.1016/j.jqsrt.2017.08.001.

18. Wang, Z., Zhang, Z.M., Quan, X., and Cheng, P. (2018). A perfect absorber design using a natural hyperbolic material for harvesting solar energy. Sol. Energy *159*, 329–336. https://doi.org/10.1016/j.solener.2017.11.002.

19. Wang, Z., Liu, Z., Zhang, C., Yang, D., Cheng, P., and Shuai, Y. (2022). Notched nanoring wideband absorber for total solar energy harvesting. Sol. Energy *243*, 153–162. https://doi.org/10.1016/j.solener.2022.07.026.

20. Jiang, C., Shan, S., Zhou, Z., Liang, L., and Huang, H. (2019). Theoretical study of multilayer ring metamaterial emitter for a low bandgap TPV cell. Sol. Energy *194*, 548–553. https://doi.org/10.1016/j.solener.2019.10.074.

21. Datas, A., Chubb, D., and Veeraragavan, A. (2013). Steady state analysis of a storage integrated solar thermophotovoltaic (SISTPV) system. Sol. Energy *96*, 33–45. https://doi.org/10.1016/j.solener.2014.07.005.

22. Tu, Y., Wu, J., Xu, G., Yang, X., Cai, R., Gong, Q., Zhu, R., and Huang, W. (2021). Perovskite solar cells for space applications: progress and challenges. Adv. Mater. *33*, 2006545. https://doi.org/10.1002/adma.202006545.

23. Wen, S., Wang, C., Zhou, Y., Duan, L., Wei, Q., Yang, S., and Shi, Y. (2019). High-density tungsten fabricated by selective laser melting: densification, microstructure, mechanical and thermal performance. Opt Laser. Technol. *116*, 128–138. https://doi.org/10.1016/j.optlastec.2019.03.018.

24. Liang, Q., Yin, Q., Chen, L., Wang, Z., and Chen, X. (2020). Perfect spectrally selective solar absorber with dielectric filled fishnet tungsten grating for solar energy harvesting. Sol. Energy Mater. Sol. Cells *215*, 110664. https://doi.org/10.1016/j.solmat.2020.110664.

25. Wang, Z., Liu, Z., Duan, G., Fang, L., and Duan, H. (2022). Ultrahigh broadband absorption in metamaterials with electric and magnetic polaritons enabled by multiple materials. Int. J. Heat Mass Transf. *185*, 122355. https://doi.org/10.1016/j.ijheatmasstransfer.2021.122355.

26. Engwall, A., Shin, S., Bae, J., and Wang, Y. (2019). Enhanced properties of tungsten films by high-power impulse magnetron sputtering. Surf. Coat. Technol. *363*, 191–197. https://doi.org/10.1016/j.surfcoat.2019.02.055.

27. Vieu, C., Carcenac, F., Pépin, A., Chen, Y., Mejias, M., Lebib, A., Manin-Ferlazzo, L., Couraud, L., and Launois, H. (2000). Electron beam lithography: resolution limits and applications. Appl. Surf. Sci. *164*, 111–117. https://doi.org/10.1016/S0169-4332(00)00352-4.

28. Areed, N.F.F., El-Wasif, Z., and Obayya, S.S.A. (2018). Nearly perfect metamaterialplasmonic absorbers for solar energy applications. Opt. Quant. Electron. *50*, 197. https://doi.org/10.1007/s11082-018-1464-6.

29. Shanks, K., Ferrer-Rodriguez, J.P., Fernández, E.F., Almonacid, F., Pérez-Higueras, P., Senthilarasu, S., and Mallick, T. (2018). A> 3000 suns high concentrator photovoltaic design based on multiple Fresnel lens primaries focusing to one central solar cell. Sol. Energy *169*, 457–467. https://doi.org/10.1016/j.solener.2018.05.016.

30. Song, M., Yu, H., Hu, C., Pu, M., Zhang, Z., Luo, J., and Luo, X. (2013). Conversion of broadband energy to narrowband emission through double-sided metamaterials. Opt Express *21*, 32207–32216. https://doi.org/10.1364/OE.21.032207.

31. Zhou, Z., Sakr, E., Sun, Y., and Bermel, P. (2016). Solar thermophotovoltaics: reshaping the solar spectrum. Nanophotonics *5*, 1–21. https://doi.org/10.1515/nanoph-2016-0011.

32. Liu, Z., Duan, G., Duan, H., and Wang, Z. (2022). Nearly perfect absorption of solar energy by coherent of electric and magnetic plasmons. Sol. Energy Mater. Sol. Cells *240*, 111688. https://doi.org/10.1016/j.solmat.2022.111688.

33. Qiu, Y., Xu, M., Li, Q., Huang, R., and Wang, J. (2021). A high-temperature near-perfect solar selective absorber combining tungsten nanohole and nanoshuriken arrays. ES Energy Environ. *13*, 77–90. https://doi.org/10.30919/esee8c482.

34. Kim, T.Y., Kim, H.K., Ku, J.W., and Kwon, O.C. (2017). A heat-recirculating combustor with multiple injectors for thermophotovoltaic power conversion. Appl. Energy *193*, 174–181. https://doi.org/10.1016/j.apenergy.2017.02.040.

35. Lang, S., Drück, H., and Bestenlehner, D. (2021). Ultrahigh temperature thermal insulation. In Ultra-High Temperature Thermal Energy Storage, Transfer and Conversion (Woodhead Publishing), pp. 201–219.

36. Sakurai, A., Zhao, B., and Zhang, Z.M. (2015). Effect of polarization on dual-band infrared metamaterial emitters or absorbers. J. Quant. Spectrosc. Radiat. Transf. *158*, 111–118. https://doi.org/10.1016/j.jqsrt.2014.11.018.

37. Maremi, F., Lee, N., Choi, G., Kim, T., and Cho, H. (2018). Design of multilayer ring emitter based on metamaterial for thermophotovoltaicapplications. Energies *11*, 2299–2306. https://doi.org/10.3390/en11092299.

38. Robitaille, P. (2003). On the validity of Kirchhoff's law of thermal emission. IEEE Trans. Plasma Sci. *31*, 1263–1267. https://doi.org/10.1109/TPS.2003.820958.

39. Chen, B., Shan, S., Liu, J., and Zhou, Z. (2022). An effective design of thermophotovoltaicmetamaterial emitter for medium-temperature solar energy storage utilization. Sol. Energy *231*, 194–202. https://doi.org/10.1016/j.solener.2021.11.067.

40. Bendelala, F., Cheknane, A., and Hilal, H. (2018). Enhanced low-gap thermophotovoltaic cell efficiency for a wide temperature range based on a selective meta-material emitter. Sol. Energy *174*, 1053–1057. https://doi.org/10.1016/j.solener.2018.10.006.

41. Chen, B., Shan, S., and Liu, J. (2022). A novel molten salt energy storage-solar thermophotovoltaic integrated system with mid-temperature metamaterial spectrum reshaping. Sol. Energy Mater. Sol. Cells *243*, 111799. https://doi.org/10.1016/j.solmat.2022.111799.

42. Shoaei, E. (2016). Performance assessment of thermophotovoltaic application in steel industry. Sol. Energy Mater. Sol. Cells *157*, 55–64. https://doi.org/10.1016/j.solmat.2016.05.012.

43. Hu, Y., Li, M., He, J.J., and LaPierre, R.R. (2013). Current matching and efficiency optimization in a two-junction nanowire-on-silicon solar cell. Nanotechnology *24*, 065402. https://doi.org/10.1088/0957-4484/24/6/065402.

44. Chan, W., Huang, R., Wang, C., Kassakian, J., Joannopoulos, J., and Celanovic, I. (2010). Modeling low-bandgapthermophotovoltaic diodes for high-efficiency portable power generators. Sol. Energy Mater. Sol. Cells *94*, 509–514. https://doi.org/10.1016/j.solmat.2009.11.015.

STAR★METHODS

KEY RESOURCES TABLE

REAGENT or RESOURCE	SOURCE	IDENTIFIER
Software and algorithms		
MATLABR2020a	The MathWorks, Inc.	https://ww2.mathworks.cn/
Origin 2019b	OriginLab	https://www.originlab.com/

RESOURCE AVAILABILITY

Lead contact

Further information and requests for resources should be directed to and will be fulfilled by the lead contact, Shiquan Shan (shiquan1204@zju.edu.cn).

Materials availability

This study did not generate new unique materials.

Data and code availability

Relevant data sources for modeling are provided in the paper.

Any additional information required to reanalyze the data reported in this paper is available from the lead contact upon request.

METHOD DETAILS

Radiation characteristics calculations

Finite difference time domain (FDTD) method[36] is used to obtain the radiation characteristics of the above micro-nano structures. The scattering parameter (S-parameter) by incident plane electromagnetic wave is obtained. The absorptance/emittance of the structure is calculated as[37]:

$$\varepsilon(\lambda) = \alpha(\lambda) = 1 - |S_{11}|^2 - |S_{21}|^2 \quad \text{(Equation 1)}$$

where$\varepsilon(\lambda)$ and $\alpha(\lambda)$ is the emittance and absorptance of the structure at λ, S_{11} is the reflection coefficient, and S_{21} is the transmission coefficient. Considering the electromagnetic wave is difficult to propagate through the structure, we default that S_{21} is 0, and the calculation can be further simplified as[37]:

$$\varepsilon(\lambda) = \alpha(\lambda) = 1 - |S_{11}|^2 \quad \text{(Equation 2)}$$

The scattering parameter is also used to obtain the effective impedance Z of the micro-nano structure. The specific calculation equation is:

$$Z = \sqrt{\frac{(1+S_{11})^2 - {S_{21}}^2}{(1-S_{11})^2 - {S_{21}}^2}} = Re(Z) + Im(Z)\cdot i \quad \text{(Equation 3)}$$

By analyzing the real part $Re(Z)$ and imaginary part $Im(Z)$ of the effective impedance, the impedance matching between the micro-nano structure and the free space can be reflected. It can provide a microscopic mechanism explanation for the radiation characteristics of the micro-nanostructure.[16]

Performance analysis

Solar radiation absorption

To obtain the solar absorption performance of the selective absorber, thermal equilibrium analysis is first conducted and the energy balance relationship is:

$$q_{abs} = q_{solar} - q_{ref} - q_{rad,loss} \quad \text{(Equation 4)}$$

$$q_{ref} = \gamma q_{solar} \quad \text{(Equation 5)}$$

$$\alpha + \gamma = 1 \quad \text{(Equation 6)}$$

where q_{abs} is the energy absorbed by the absorber, q_{solar} is the space solar radiation energy, q_{ref} is the energy reflected by the absorber, $q_{rad,loss}$ is the radiation heat loss of the absorber, α, γ are the absorptivity and reflectivity of the absorber, respectively. By integrating the above equations, the relations can be expressed as:

$$q_{abs} = \alpha q_{solar} - q_{rad,loss} \quad \text{(Equation 7)}$$

Based on the AM0 solar radiation and the absorber absorptance distribution at different wavelengths, it can be further expressed as:

$$q_{solar} = \int_{400nm}^{4000nm} C G_{solar}(\lambda) d\lambda \quad \text{(Equation 8)}$$

$$q_{abs} = \int_{400nm}^{4000nm} C\alpha(\lambda) G_{solar}(\lambda) - \varepsilon(\lambda) E_b(\lambda, T_a) d\lambda \quad \text{(Equation 9)}$$

where C is the concentration ratio, λ is the wavelength, $G_{solar}(\lambda)$ is the solar radiation intensity at λ, $T_a$is temperature of the absorber, $E_b(\lambda, T_a)$ is the blackbody emission intensity at λ and T_a, $\alpha(\lambda)$, $\varepsilon(\lambda)$ are the spectral absorptance and emittance of the absorber at λ. According to Kirchhoff's law,[38] $\alpha(\lambda) = \varepsilon(\lambda)$ at thermal equilibrium,q_{abs} can be calculated as:

$$q_{abs} = \int_{400nm}^{4000nm} \alpha(\lambda)[C G_{solar}(\lambda) - E_b(\lambda, T_a)] d\lambda \quad \text{(Equation 10)}$$

On this basis, the solar absorption efficiency η_{abs} and total absorptanceα_{tot} of the absorber to the AM0 radiation by the selective absorber η_{abs} can be calculated as[16]:

$$\eta_{abs} = \int_{400nm}^{4000nm} \alpha(\lambda) \left(1 - \frac{E_b(\lambda, T_a)}{C G_{solar}(\lambda)}\right) d\lambda \quad \text{(Equation 11)}$$

$$\alpha_{tot} = \int_{400nm}^{4000nm} \frac{\alpha(\lambda) G_{solar}(\lambda) d\lambda}{G_{solar}(\lambda) d\lambda} \quad \text{(Equation 12)}$$

During the geometrical parameters optimization of the absorber, a highest solar absorption efficiency is aim to be obtained to ensure the energy input of the space STPV system.

TPV heat-electric conversion

Reshaping of the AM0 spectrum is the key of the proposed system. At the backend of the system, the generation of a thermal spectrum with high matching degree with PV cell by the selective emitter is another important step before the final electrical power generation. Therefore, The spectral regulation performance of the selective emitter is evaluated with spectral efficiency η_{spec} , which is defined as[39]:

$$\eta_{spec} = \frac{\int_0^{\lambda_c} E_b(\lambda, T_e) \varepsilon_e(\lambda) d\lambda}{\int_0^{\infty} E_b(\lambda, T_e) \varepsilon_e(\lambda) d\lambda} \quad \text{(Equation 13)}$$

where λ_c is the cut-off wavelength of the Si/InGaAsSb tandem cell, $\varepsilon_e(\lambda)$ is the emittance of the emitter at λ, and T_e is the temperature of the emitter.

On this basis, the TPV power generation performance of the backend of the system can be further analyzed. First, the thermal radiation energy of the emitter q_{rad} is calculated as:

$$q_{rad} = \int_0^{\infty} E_b(\lambda, T_e) \varepsilon_e(\lambda) d\lambda \quad \text{(Equation 14)}$$

With the spectrum reshaping of the selective emitter, the generated thermal radiation is then converted into electricity by the Si/InGaAsSb tandem cell, and the generated electrical energy P_{el} and TPV efficiency η_{tpv} is calculated as[40,41]:

$$P_{el} = \int_0^\infty V_{OC} \cdot FF \cdot \frac{q_0 \lambda}{hc} EQE(\lambda) \varepsilon_e(\lambda) E_b(\lambda, T_e) d\lambda \quad \text{(Equation 15)}$$

$$\eta_{tpv} = \frac{P_{el}}{q_{rad}} \quad \text{(Equation 16)}$$

where FF is the fill factor, q_0 is the elementary charge, h is Planck's constant, c is the speed of light, and $EQE(\lambda)$ is the external quantum efficiency of the Si/InGaAsSb tandem cell at λ, V_{OC} is the open-circuit voltage, which is calculated as[42]:

$$V_{oc} = \frac{\Gamma k T_c}{q_0} \ln\left(\frac{J_{sc}}{J_0} + 1\right) \quad \text{(Equation 17)}$$

where Γ is the diode ideality factor (taken as 1), k is the Boltzmann constant, and T_c is the cell temperature, which is set as 300 K. The saturation current J_0 is shown as[42]:

$$J_0 = 1.5 \times 10^5 \exp\left(-\frac{E_g}{kT_c}\right) \quad \text{(Equation 18)}$$

where E_g is the band gap of the PV cell, which is taken as 1.1 eV for Si cell[43] and 0.5548 eV for InGaAsSbcell.[44]

The fill factor FF is calculated as[42]:

$$FF = \beta \frac{\nu - \ln(\nu + 0.72)}{\nu + 1} \quad \text{(Equation 19)}$$

$$\nu = \frac{q_0 V_{oc}}{kT_c} \quad \text{(Equation 20)}$$

where β is the correction factor, which is set as 0.96.

During the geometrical parameter optimization of the emitter, a highest TPV efficiency is aim to be obtained to ensure the efficient utilization of the absorbed solar energy.

Overall system performance

To evaluation the utilization efficiency of the AM0 solar radiation by the overall space STPV system, the STPV system efficiency η_{sys} is calculated by coupling the influence of different ends as:

$$\eta_{sys} = \eta_{abs} \eta_{tpv} \quad \text{(Equation 21)}$$

To analyze the structural rationality of the system, considering the thermal equilibrium between the emitter and the absorber, the area ratio of the absorber and the emitter is obtained as:

$$\frac{A_{abs}}{A_{emi}} = \frac{q_{rad}}{q_{abs}} \quad \text{(Equation 22)}$$

where A_{abs} is the absorber area and A_{emi} is the emitter area.